Hindawi
Journal of Advanced Transportation
Volume 2022, Article ID 5951389, 9 pages
https://doi.org/10.1155/2022/5951389

Research Article

The Improved Precoding Method in the VLC-Based Intelligent Transportation System

Shilin li,[1] **Y. Cheng**,[1] **T.Y. Zhou**,[1,2] **and P.Y. Liang**[1]

[1]*School of Information, Hunan University of Humanities, Science and Technology, Loudi 417000, China*
[2]*School of Electronics and Information, Northwestern Polytechnical University, Xi'an 710129, China*

Correspondence should be addressed to Y. Cheng; yuncheng@huhst.edu.cn and T.Y. Zhou; taoyun_2000@163.com

Received 29 April 2022; Revised 1 June 2022; Accepted 14 June 2022; Published 30 June 2022

Academic Editor: Zhenzhou Yuan

Visible light communication (VLC) transmission system, combined with lighting and communication, has a great application value in the field of intelligent transportation. To efficiently improve the performance of VLC-based intelligent transportation system, an improved precoding scheme is proposed and experimentally verified. Partial data-carrying subcarrier (PDS)-precoding scheme can balance the signal-to-noise ratio (SNR) and combat frequency selective fading (FSF) in the VLC-based intelligent transportation system. For ~3.52 Gb/s DMT-VLC system with 1.9-m free space transmission, the OCT-based PDS-precoding signal shows almost the same BER performance as full data-carrying subcarriers precoding ones. Compared with the conventional scheme, the BER is reduced from 2e-3 to 8.14e-5 by using the proposed PDS-precoding. PDS-precoding is a nice choice to degrade the unbalanced damage for data-carrying subcarriers (SCs) in the bandwidth-limited VLC-based intelligent transportation system.

1. Introduction

Visible light communication (VLC)-based intelligent transportation communication system has received extensive research owing to the possibility of integration of lighting, traffic indication, and communication [1, 2]. The application scenario diagram of the VLC communication system for intelligent transportation (see Figure 1).

The VLC-based intelligent transportation communication system can be more efficiently applied in V2V scenario and so on, owing to the improvement of the performance. The VLC-based intelligent transportation communication system is rich in spectrum resources (380 THz ~ 780 THz), which is about 10000 times than that of the RF spectrum (300 kHz ~ 30 GHz). Besides, VLC combines lighting and communication and has broad economic prospects, so it has been widely studied in [3–5]. The concept of VLC was proposed in [6] by the Japanese scholars in 2000 and was firstly used to transmit data for indoor communication links. The Visible Light Communication Consortium (VLCC) which was the first international organization on VLC was established in Japan in 2003. VLC experimental verification with a rate of 10 Mbps was completed by the Japanese research team in 2004 [7]. Sugiyama of Keio University in Japan realized visible light transmission with 96 Mbps through Pulse Position Modulation (PPM) [8]. In 2009, Vucic et al. in Germany further increased the transmission rate of VLC to 230 Mbps based on the discrete multi-tone (DMT) and bit loading technique over a transmission distance of 0.7 m [9]. Fujimoto et al. [10] increased the LED bandwidth from −3 dB to 180 MHz with hardware equalization technology in 2014, which realized 662 Mbps, 600 Mbps, and 520 Mbps signal transmission rate with blue LED, red LED, and green LED with the On Off Keying (OOK) modulation technique, respectively. Chi Nan team in [11] carried out Wavelength Division Multiplexing (WDM) on the experimental LED to realize the transmission of 10.72 Gbps with high-order quadrature amplitude modulation (QAM) and DMT modulation in 2018, which was the highest transmission rate of the VLC system at that time. In 2020, the key laboratory of electromagnetic wave information science of Fudan University proposed a single input

Figure 1: The application scenario diagram of the VLC communication system for intelligent transportation.

and multiple output VLC system for vehicle networking, which could achieve a transmission rate of more than 1 Gbps at the communication distance of 4 meters by using the headlights as the transmitting end and adopting a neural network deep learning equalizer. It was the first VLC transmission system with a transmission rate of more than 1 Gbps with the industrial headlights [12]. However, the limited modulation bandwidth is the main obstacle for the ready-made LDS VLC system to achieve high transmission capacity [13–15]. Discrete Multi Tone (DMT) is used in the VLC system as a special hyperspectral efficiency modulation format. At present, the unbalanced signal-to-noise ratio (SNR) distribution of subcarriers (SCs) caused by frequency selective fading is a key issue to limit the achievable capacity of the VLC system, and the adaptive modulation method is considered to be one of the classic and effective methods to solve the problem, including adaptive bit and/or power load [16]. At the same time, scholars proposed the preemphasis [17] and postequalization [18] schemes based on electronic circuit or digital processing. However, adaptive load DMT and equalization schemes are channel dependent, and the channel state information needs to be fed back on all data-carrying subcarriers through the reverse link, which greatly limits their application in channel time-varying scenarios.

To implement a robust VLC-based intelligent transportation system [19, 20], the precoding method which is independent from channels/signals can realize data transmission reliably in various physical channel scenarios. The mapped DMT symbol is coded by multiplying the precoding matrix for Digital Signal Processing (DSP) at the DMT-enabled transmitter. At the DMT-enabled receiver, the mapped DMT symbol is decoded by the inverse of the precoding matrix [21]. In the following paragraph, we name this method as full data subcarriers (FDS)-precoding method. As mentioned in [22], the same signal-to-noise ratio distribution over full SCs after FDS-precoding can be done when the coefficient representing the signal amplitude in the FDS-precoding matrix are equal. Y. Hong et al. propose that the OCT-enabled FDS-precoding method shows a better BER/SNR performance than discrete the Fourier transform (DFT)-enabled FDS-precoding method in the VLC communication system to combat the effect of frequency-selective fading. To further improve the system capacity, [23]we proposed a 256 QAM OFDM modulation scheme coded with bit interleaved polar based on OCT precoding. M. Chen et al. in [24] had fully studied the comparison of different precoding methods from the Peak-to-Average Power Ratio (PAPR), tolerance of nonlinear distortion, computational complexity and BER performance, and so on and showed that the FDS-precoding method based on the complex valued OCT had a high computational complexity.

To efficiently combat the severe frequency selective fading of miscrete multi-tone (DMT) in the VLC-based intelligent transportation system, a channel-independent Orthogonal Circular Matrix Transform (OCT)-enabled Partial Data-carrying Subcarriers (PDS)-precoding scheme is proposed and experimentally verified. The rest of the paper is organized as follows: in Section 2, firstly, the principle of several classic precoding schemes (e.g. DFT/DHT/DST/DCT) is introduced, and the relative block diagram of DSP processing is also shown; secondly, the principle of FDS-precoding/PDS-precoding scheme is analyzed; in Section 3, the LD-based VLC experimental system is constructed; in Section 4, the relative experimental results are discussed; in Section 5, we conclude our work.

2. Principles

2.1. Classical Precoding Technology in the VLC-Based Intelligent Transportation System. Before the construction of signals with Hermite symmetry, the input constellation mapping symbol sequence is processed with a preset precoding matrix to achieve the PAPR suppression in classical precoding technology. The signal processing principle of precoding technology in the VLC system (see Figure 2).

After constellation mapping and S/P conversion, the input signal outputs an N-point symbol sequence $A = [A_0, A_1, \ldots, A_{N-1}]^T$, which is then processed by a precoding matrix P of $N \times N$ size and outputs the encoded sequence of N points $X = [X_0, X_1, \ldots, X_{N-1}]^T$.

$$\begin{aligned} X &= [X_0, X_1, \ldots, X_{N-1}]^T \\ &= \begin{bmatrix} P_{0,0} & P_{0,1} & \cdots & P_{0,N-1} \\ P_{1,0} & P_{1,1} & \cdots & P_{1,N-1} \\ \vdots & \vdots & \ddots & \vdots \\ P_{N-1,0} & P_{N-1,1} & \cdots & P_{N-1,N-1} \end{bmatrix} A \\ &= [A_0, A_1, \ldots, A_{N-1}]^T, \end{aligned} \tag{1}$$

where X_i is the element of X sequence, which is depicted as

$$X_i = \sum_{m=0}^{N-1} P_{i,m} A_m \quad 0 \le i \le N-1, \tag{2}$$

where i and m represent the ith row and mth column, respectively.

In classical precoding technology, **P** is a matrix based on unitary transformation, such as the DFT matrix, DHT matrix, DCT matrix and DST matrix, and so on.

Let

$$P = G \cdot U, \tag{3}$$

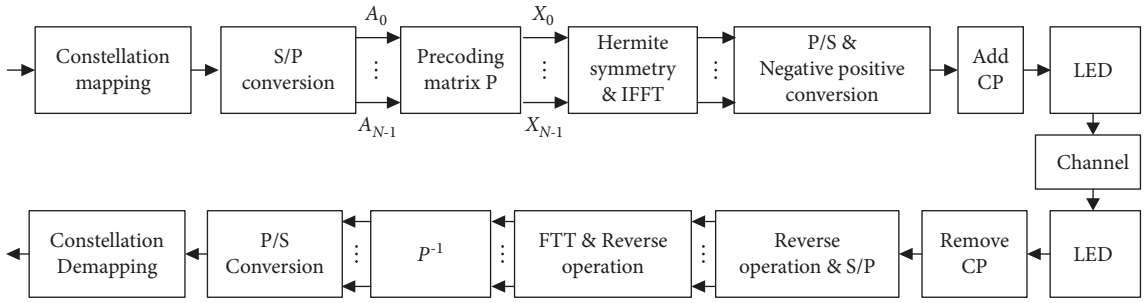

Figure 2: The structure chart of classical precoding technology in the VLC-based intelligent transportation system.

where G is the coefficient matrix corresponding to the unitary transformation matrix, and U is the corresponding unitary kernel matrix.

The unitary core element DFT, DHT, DST, and DCT precoding matrix is represented as equations (4)–(7), respectively.

$$\{U_{\mathrm{DFT}}\}_{i,m} = \exp\left[-j2\pi\left(\frac{im}{N}\right)\right] \quad 0 \le i, m \le N-1, \tag{4}$$

$$\{U_{DHT}\}_{i,m} = \cos\left(\frac{2\pi im}{N}\right) + \sin\left(\frac{2\pi im}{N}\right) \quad 0 \le i, m \le N-1, \tag{5}$$

$$\{U_{DST}\}_{i,m} = \sin\left(\frac{\pi(i+1)(m+1)}{N+1}\right) \quad 0 \le i, m \le N-1, \tag{6}$$

$$\{U_{\mathrm{DCT}}\}_{i,m} = \cos\left(\frac{\pi i(2m+1)}{2N}\right) \quad 0 \le i, m \le N-1. \tag{7}$$

Like other VLC systems, the precoded signal is transmitted from the LED to the receiving end with some corresponding operations. At the receiving end, an inverse operation is performed with the received signals and then is processed with the inverse matrix of the precoding matrix **P** during the decoding operation. Finally, the original signal is recovered by constellation demapping. Precoding and its inverse operation itself do not cause any signal loss, so precoding is a distortion-free technology.

2.2. FDS-Precoding Method. At the DMT-enabled transmitter, **M**th modulated QAM symbol can expressed as $\mathbf{x} = [x_1, x_2, ..., x_N]$. In this work, the average power of QAM mapped with DMT symbols is normalized with a normalization factor, which is $\sqrt{10}$ for the 16-QAM modulation. According to [24], the FDS-precoding matrix **Q** is written as

$$Q = \begin{bmatrix} Q_{1,1} & Q_{1,2} & \cdots & Q_{1,N} \\ Q_{2,1} & Q_{2,2} & \cdots & Q_{2,N} \\ \vdots & \vdots & \ddots & \vdots \\ Q_{N,1} & P_{N,2} & \cdots & Q_{N,N} \end{bmatrix} \cdot N^{-1/2}, \tag{8}$$

where **M** equals to **N** which denotes data-carrying SC number. Thus, the FDS-precoding matrix **Q** is an orthogonal matrix. After the processing of inverse fast Fourier transform (IFFT), the real valued precoded DMT symbol can be expressed as **Q**·**x**. Then, the transposed FDS-precoding matrix is satisfied with the following relationship:

$$R^T = Q \cdot x^T, \tag{9}$$

where $\mathbf{R} = [r_1, r_2, ..., r_N]$ is the FDS-enabled precoded DMT symbols. $[\cdot]^{\mathrm{T}}$ represents the transpose operation of the matrix. According to [25], after the processing of IFFT, the FDS-precoding **N**-QAM DMT symbol is given by

$$c(m) = M^{1/2} \sum_{\substack{i=-N \\ i \neq 0}}^{N} r_i e^{j2\pi km/M}, \tag{10}$$

where **M** is FFT-IFFT size, i.e., $m \in [1, \mathbf{M}-1]$ and is an integer. It should be noted that $r_{-\mathrm{i}}$ is the complex conjugate of r_{i}. According to equation (10), after **M**-point IFFT, the average peak-to-peak power of each SC reaches $\mathbf{M}^{-1}$.Thus, the power of the PDS-precoding DMT signal can reach $2\mathbf{N}\cdot\mathbf{M}^{-1}$.

2.3. PDS-Precoding Method. Different from the characteristics of the additive white Gaussian noise channel (AWGN), in free space channel, the data SCs suffer from the effect of frequency selective fading. The relationship between the SNR and the data subcarrier index of the VLC system is qualitatively analyzed (see Figure 3), from which we can know that the frequencies of the LD and electronic amplifier (EA) are imperfect, resulting in low signal-to-noise ratio of low-frequency data subcarriers, i.e., $1 \sim N_n$ th. Due to the bandwidth limitation of AWG [24] and LD [26], the signal-to-noise ratio of the high frequency data subcarrier, i.e., $K_1 \sim K_l$ th, decreases seriously. Different from the traditional full data subcarrier (FDS) precoding scheme, only partial data subcarriers, i.e., $0 \sim N_n^{\mathrm{th}}$, $L_1 \sim L_l^{\mathrm{th}}$, and $K_1 \sim K_k^{\mathrm{th}}$, (see Figure 3(a), 3(b), and 3(d)) are used to realize the SNR balance of the QAM-modulated VLC-based intelligent transportation system.

2.4. OCT-Enabled Scheme. The OCT-enabled FDS-precoding matrix **Q** can be expressed as

$$Q_{\mathrm{OCT}}^{x,y} = e^{-j2\pi(x-1)(y-1)/N}, \tag{11}$$

where **x** or **y** represents the row- or column-index of the OCT precoding matrix, respectively and ranges from 1 to **N**.

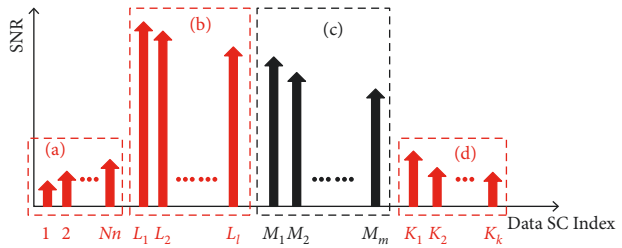

FIGURE 3: The qualitative analysis of the relationship between the SNR and the SC index in the VLC-based intelligent transportation system.

j equals to $\sqrt{-1}$. The key elements for the OCT-based precoding scheme are OCT-based matrice construction. Different values of parameter in Zadoff–Chu sequence, i.e., **O**, determine the different OCT-based matrice construction method. According to [27],

when **O** is even, the **M**th element in Zadoff–Chu sequence satisfies

$$n_m = e^{j2\pi w/O\left((m-1)^2/2+z(m-1)\right)}. \tag{12}$$

When **O** is odd, the **M**th element in Zadoff–Chu sequence follows

$$n_m = e^{j2\pi w/O\left((m-1)m/2+z(m-1)\right)}, \tag{13}$$

where m and z are all integers, $m\in[1, M-1]$. In addition, w is prime to O which equals to N^2. According to equation (11)–(13), when $x-y+1>1$, the matrix, i.e., $Q_{\mathrm{OCT}}^{x,y}$, are constructed by $C_{x\text{-}y+1}$. When $x-y+1\le 1$, t w the matrix, i.e. $Q_{OCT}^{x,y}$, are constructed by $C_{x\text{-}y+1}+x$.

2.5. SNR Balanced over SCs. At the DMT-enabled receiver, timing synchronization is realized by using a training sequence (TS) coupled with the intra-symbol frequency-domain averaging (ISFA) technique. Thus, there exists no inter-symbol interference (ISI) and inter-carrier interference (ICI) which will affect the performance of the SCs. In this section, we suppose that accurate channel estimation is achieved.

In this work, $\mathbf{Q}=[q_1, q_2, ..., q_N]$ and $v = [v_1, \cdot v_2, \ldots, \cdot v_N]$ are denoted the data vectors at the transmitter and noise vector in the frequency domain, respectively. Thus, after the processing of channel estimation, equalization, and OCT-decoding, the recovered QAM-DMT symbols, $\tilde{x} = [\tilde{x}_1, \tilde{x}_2, \ldots \tilde{x}_m]$, can be expressed as

$$\begin{aligned}\tilde{x}^T &= Q^{-1}C^{-1}\left(HR^T + v\right)\\ &= \tilde{x}^T + \tilde{v}^T,\end{aligned} \tag{14}$$

where **C** denotes the channel response matrix.$\mathbf{Q^{-1}}$ and $\mathbf{C^{-1}}$ denote the corresponding inverse matrix. Because the OCT-enabled precoded matrix **Q** is an orthogonal matrix, the result of matrix **Q** after conjugate transposition equals to $\mathbf{Q^{-1}}$. Thus, the noise vector $\tilde{v}^T$ which obeys $\tilde{v}^T \sim N(0, \overline{\sigma}_k^2)$ can be further expressed as equation (15).

$$\begin{aligned}\tilde{v}^T &= Q^{-1}C^{-1}v^T\\ &= N^{-\frac{1}{2}}\begin{bmatrix} Q_{1,1}^* & Q_{2,1}^* & \cdots & Q_{N,1}^*\\ Q_{1,2}^* & Q_{2,2}^* & \cdots & Q_{N,2}^*\\ \vdots & \vdots & \ddots & \vdots\\ Q_{1,N}^* & Q_{2,N}^* & \cdots & Q_{N,N}^*\end{bmatrix}\begin{bmatrix}\frac{1}{c_1} & 0 & \cdots & 0\\ 0 & \frac{1}{c_2} & \cdots & 0\\ \vdots & \vdots & \ddots & \vdots\\ 0 & 0 & \cdots & \frac{1}{c_N}\end{bmatrix}\begin{bmatrix}v_1\\ v_2\\ \vdots\\ v_N\end{bmatrix}\\ &= N^{-1/2}\left[\sum_{j=1}^{N}\frac{Q_{j,1}^* v_i}{c_j}, \sum_{i=1}^{M}\frac{Q_{j,2}^* v}{c_j}, \ldots, \sum_{i=1}^{M}\frac{Q_{j,N}^* v}{c_j},\right]^T\\ &= \left[\tilde{v}_1, \tilde{v}_2, \ldots, \tilde{v}_N\right]^T,\end{aligned} \tag{15}$$

where v_n denotes the noise vector on the **k**th data SCs after OCT-decoding and the operation of conjugate transpose can be expressed $[.]^*$ and $\overline{\sigma}_k^2$ as follows:

$$\overline{\sigma}_k^2 = N^{-1}\sum_{j=1}^{N}\left|\frac{Q_{j,k}^*}{c_j}\right|^2\sigma_j^2. \tag{16}$$

The normalized power of the 16-QAM-DMT signal gained from equation (10) is one. After OCT-decoding, the SNR of the **k**th subcarriers follows

$$\mathrm{SNR}_k = \frac{N}{\sum_{j=1}^{N}\left|Q_{j,k}^*/c_j\right|^2\sigma_i^2}. \tag{17}$$

Here, the error vector magnitude (EVM) is considered to follow the relationship as

$$\mathrm{EVM} = 20\log_{10}\left(\frac{\sum_{m=1}^{M}\left|e_m^2\right|}{\sum_{m=1}^{M}\left|x_m^2\right|}\right)^{1/2}, \tag{18}$$

where $\mathbf{x}_\mathbf{k}$ and x_k represent the transmitted QAM-modulated DMT symbols and received QAM-demodulated DMT symbols, respectively. **M** is the quantity of transmitted QAM-DMT symbols, e_m satisfying $e_m = \tilde{x}_m - x_m$ which denotes the error signal. In this paper, set **M**=1000×**N**=384,000.

3. Experimental Setup of the VLC-Based Intelligent Transportation Communication System

The experimental structure of the VLC-based intelligent transportation communication system (see Figure 4). A 16QAM is used at the transmitter for data mapping, which is different from the conventional DMT. The imbalance of the signal-to-noise ratio among the VLC channels before Hermitian symmetry and IFFT is mitigated with the partial

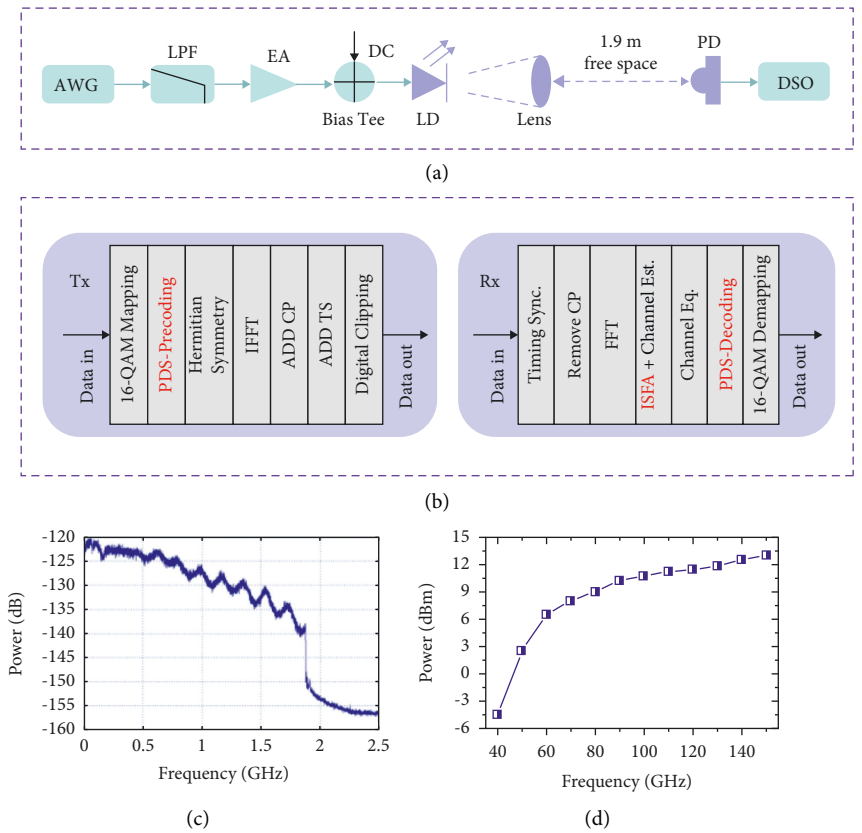

Figure 4: (a) The experimental structure diagram of the VLC-based intelligent transportation communication system; (b) the corresponding DSP; (c) the spectrum of the received DMT signal; and (d) the output power versus I Bias.

data-carrying subcarriers precoding based on the OCT scheme. Then, the ISI is removed by adding a cyclic prefix (CP) and needs only one TS inserted in PDS-precoding. Finally, before being sent to Tektronix arbitrary waveform generation (AWG), the data need to be digitally clipped. The sampling rate and resolution of the AWG are 2.5 GSa/s and 10 bit, respectively. It is worth noting that when the same peak amplitude is inserted into the system in front of the TS, the average power of the conventional DMT signal and the full/partial data-carrying subcarriers precoding DMT signals will remain the same. After the suppression of the converted high frequency image with a 1 GHz low pass filter (LPF), it is strengthened by a 4 GHz electrical amplifier (EA). In order to make the laser diode work in a linear state, it is needed to use a bias-tee and set the direct current (DC) bias 4.6 V.

At the receiver, after 1.9 m free space carrying, the signal is detected by a photodiode (PD). The received signal captured by a LeCroy digital storage oscilloscope (DSO) with 8 bit vertical resolution. The time-domain DMT signal is firstly oversampled by a sampling signal whose frequency is two times than the effective sampling rate valued 2.5 GSa/s and then converted by a DAC whose frequency is 5 GSa/s. Therefore, the gross bit rate is 3.75 Gb/s $((2.5 * 400 * 384 * 4)/1024 * 400)$, and the net bit rate is 3.52 Gb/s $((2.5 * 400 * 384 * 4)/(1024 + 64) * 401)$. The sampling signal will be postprocessed with the DSP, whose processing flow includes symbol timing synchronization based on TS, removal of cyclic prefix, FFT, frequency averaging technique among symbols and zero-forcing of channel estimation, domain equalization with one-tap frequency, decoding of partial data-carrying sub-carriers, and demapping of symbols. Finally, BER is calculated for evaluating system performance. The spectrum of the received DMT signal and the output power versus I Bias (see Figure 4(c) and 4(d)). It is worth noting that we can use bias current intensity, such as I Bias, to control the light intensity. On the one hand, a high bias current can raise the power and improve the EVM. On the other hand, a high bias current will cause a nonlinear LED effect.

4. Experimental Results and Analysis

The implementation complexity of two kinds of the precoding scheme, according to equation (9) is analyzed. The required numbers of SCs used for precoding, real multiplications, and additions are listed in Table 1. Compared with the FDS-precoding scheme, the number of SCs used for OCT-enabled matrix construction are reduced from 384 to 254 in PDS-precoding. Thus, the required real multiplications and additions are also reduced by a large margin. Thus, OCT-enabled PDS-precoding has the lower complexity.

To identify the optimal IFFT size for the VLC-based intelligent transportation system, the DMT signal without the precoding scheme is sent by the transmitter. After 1.9 m

Table 1: Implementation complexity comparison.

Item	Numbers of SCs used for precoding	Mult (N)	Add
OCT-enabled FDS-precoding	SCs: 1~384th; (N_1= 384)	4_1^2	$4N_1^2 - 2N_1$
OCT-enabled PDS-precoding	SCs: 1~160th, 291~384th; (N_2= 254)	4_2^2	$4N_2^2 - 2N_2$

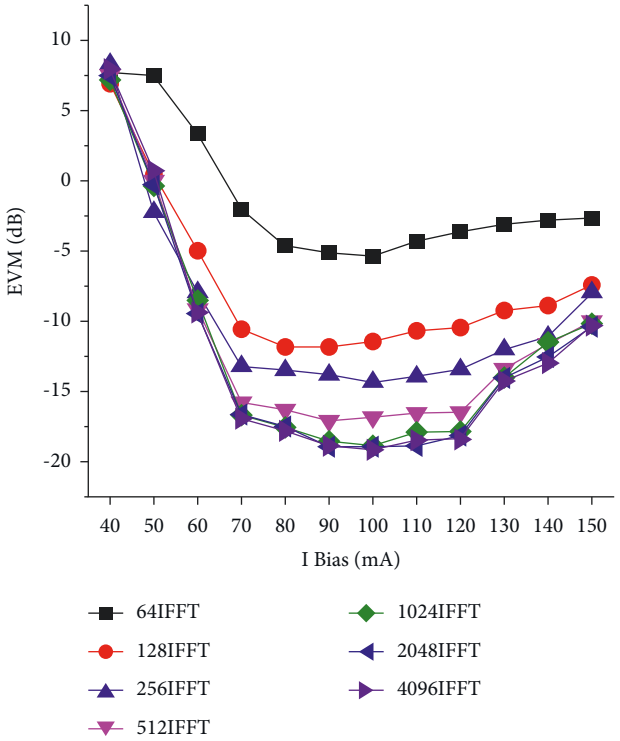

Figure 5: EVM performance versus I Bias.

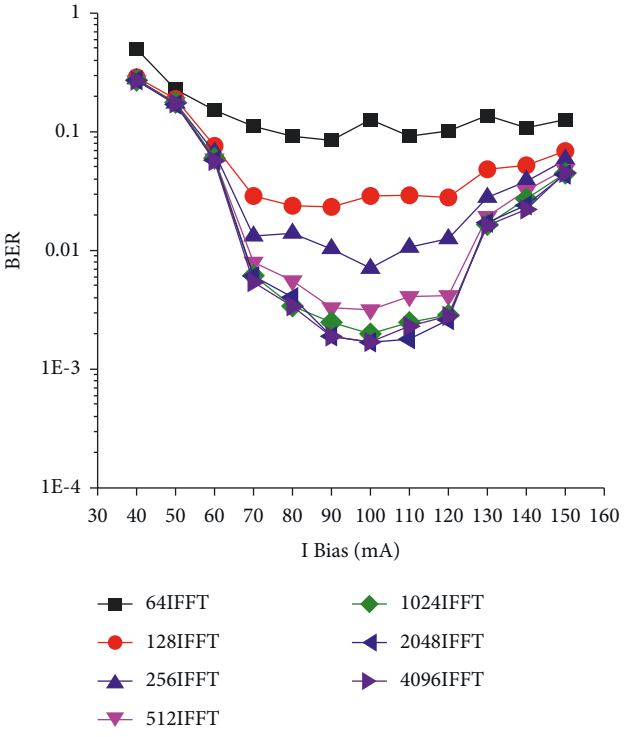

Figure 6: BER performance versus I Bias.

free space transmission, EVM and BER as a function of I Bias (see Figures 5 and 6) from which it is easy to know that the performance of EVM and BER is improved with the increase of the IFFT size. However, once the I Bias becomes larger than 100 mA, the performance of EVM and BER begins to deteriorate owing to the nonlinear impairments. So, there is an optimum performance when the I Bias ranges within 90~100 mA. There is an improvement of 13.5 dB in EVM when the IFFT increases from 64 to 4096 with a fixed I Bias at 100 mA, and the reason for this is that there is less side-lobe power leakage for the DMT signal with a large IFFT size, which is less sensitive to narrow filtering effects. When I Bias is fixed at 100 mA, the BER performance increases from $2e^{-3}$ to $1.4e^{-3}$ with the IFFT size increasing from 1024 to 4096. Considering the computational complexity and minimal performance gain, we set the IFFT size to 1024 in the following discussion:

The variation curve of the estimated SNR of different signals with the SC index (see Figure 7), where the I Bias is set to 100 mA and the peak value of the output signal from the AWG is set to 500 mV. It can be seen that with regard to the conventional DMT signals, there are unbalanced impairments in the data-carrying subcarriers, and the SNR difference between the maximum and minimum can reach 19 dB. There are low SNRs in low-frequency subcarriers, and this is because the frequency response of the LD and EA is imperfect. Similarly, there are degraded SNRs in high frequency subcarriers, and the reason for this is that the bandwidth of AWG and LD is limited. In our experiments, there are 384 data-modulated subcarriers in each DMT symbol carrier, and all the data-carrying subcarriers are used for OCT-based on the FDS-precoding scheme. The balanced SNRs over full data-carrying subcarriers are shown in Figure 7(b). Only 1~160th and 291~384th data-carrying subcarriers were used for OCT-based PDS-precoding scheme. The balanced SNRs over partial data-carrying subcarriers (see Figure 7(c)). Compared with the conventional DMT scheme, the SNRs of the precoded SCs stabilized near 18.5 dB and 18.2 dB for the FDS-precoding scheme and PDS-precoding scheme, respectively.

The performance of BER for different DMT signals after 1.9 m free space transmission versus I Bias is also investigated (see Figure 8). When the I Bias is 100 mA, the BER performance of the proposed PDS-precoding scheme can be improved by more than one order of magnitude compared with the conventional scheme. The BERs of FDS-precoding scheme and PDS-precoding scheme are $8.3e^{-5}$ and $8.14e^{-5}$, respectively. The numerical difference of the BER is very small, but the implementation complexity reduces by about 34 percent.

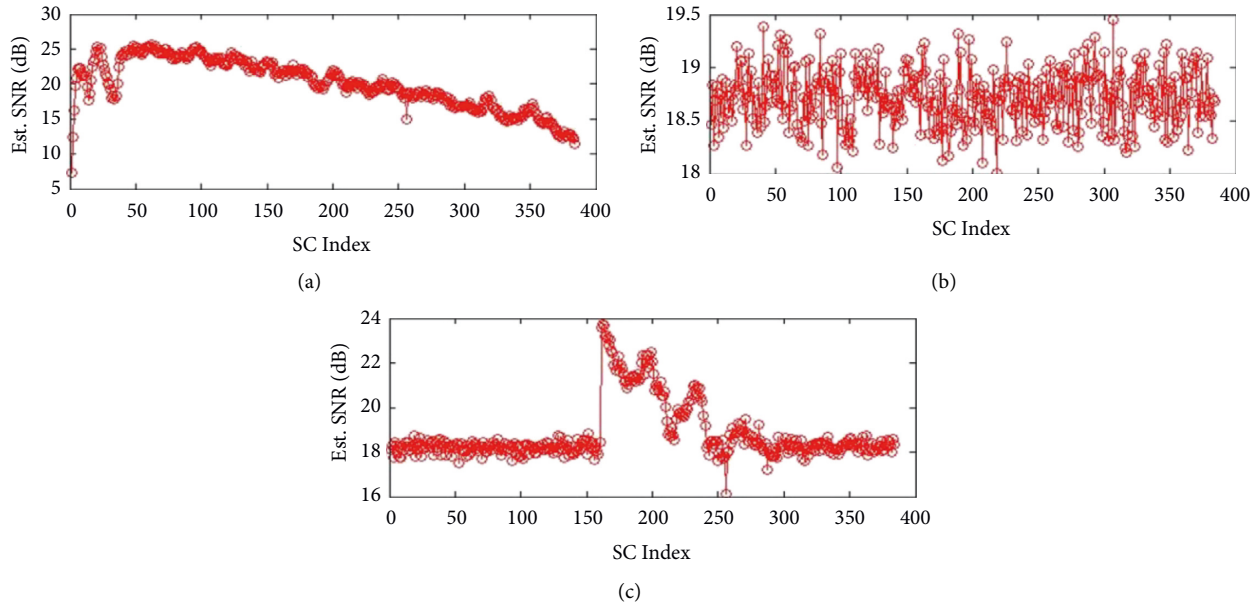

Figure 7: The variation curve of the estimated SNR of different signals with the SC index (a) conventional, (b) FDS-precoding, and (c) PDS-precoding.

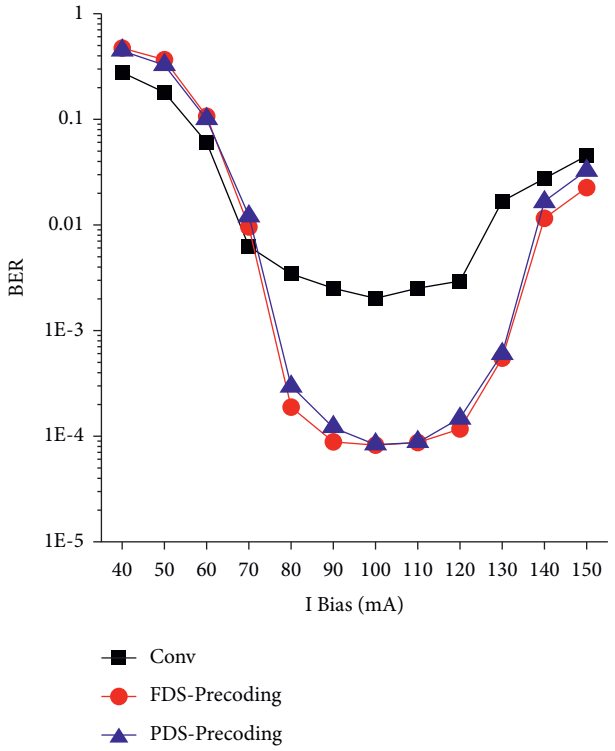

Figure 8: The BER performances versus I Bias for different DMT signals.

The constellation diagrams of the recovered 16QAM and their EVM values (see Figure 9), from which it is easy to see that there is a minor improvement in the EVM performance, benefit from the PAPR reduction of the precoding methods compared with the conventional DMT signals. In summary, PDS-precoding is one of the best choices to offset the unbalanced impairments in the VLC-based intelligent transportation system whose bandwidth is limited, and it can improve the BER performance and reduce the implementation complexity effectively.

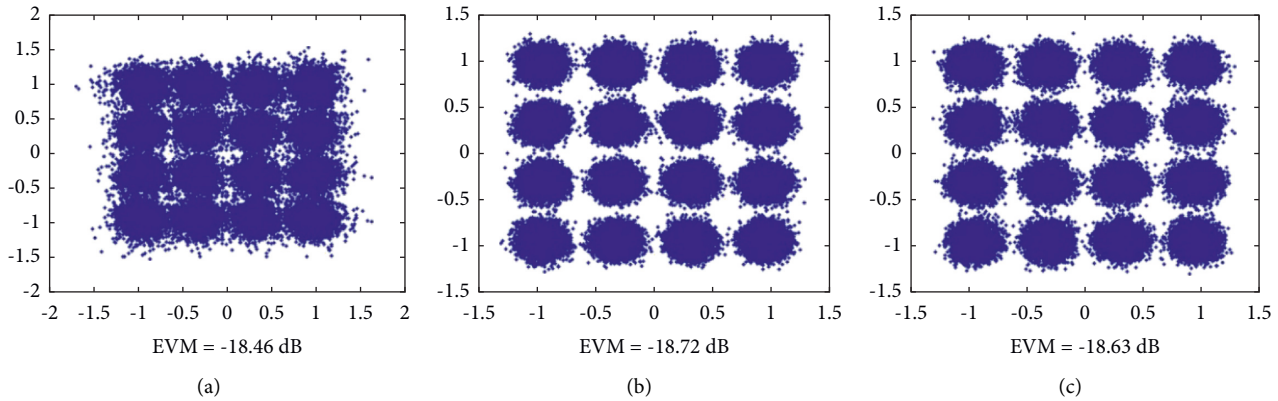

Figure 9: Constellation diagrams of the recovered 16QAM and their EVM values. (IFFT= 1024, I Bias= 100 mA). (a) Conventional (b) FDS-precoding (c) PDS-precoding.

5. Conclusions

In this paper, a fast OCT-based PDS-precoding technique is proposed in the VLC-based intelligent transportation communication system. For ~3.52 Gb/s VLC-based intelligent transportation system with 1.9 m free space transmission, compared with FDS-precoding method, the PDS-precoding scheme shows the similar BER performance as FDS-precoding ones, and the implementation complexity reduces by about 34 percent. Compared with the conventional scheme, the BER performance is reduced from $2e^{-3}$ to $8.14e^{-5}$ by using PDS-precoding. PDS-precoding is one of the best choices to offset the unbalanced impairments in the VLC-based intelligent transportation system whose bandwidth is limited, and it can improve the BER performance and reduce the implementation complexity effectively.

Data Availability

The data used to support the findings of this study are included within the article.

Conflicts of Interest

The authors declare that there are no conflicts of interest regarding the publication of this paper.

Acknowledgments

This work was supported by the Construct Program of the Key Discipline in Hunan Province, China,the Aid program for Science and Technology Innovative Research Team in Higher Educational Institute of Hunan Province, China and the Scientific Research Fund of Hunan Provincial Education Department of China (21A0562).

References

[1] Y. Yang, K. He, Y.-p. Wang, and Z.-z.Y.-h.M.-z. Yuan, "Identification of dynamic traffic crash risk for cross-area freeways based on statistical and machine learning methods," *Physica A: Statistical Mechanics and Its Applications*, vol. 595, Article ID 127083, 2022.

[2] Y. Yang, Z. Yuan, and R. Meng, "Exploring traffic crash occurrence mechanism towards cross-area freeways via an improved data mining approach," *Journal of Transportation Engineering Part A Systems*, 2022.

[3] N. Chi, *Key Technologies of High Speed Visible Light Communication*, pp. 222-223, Posts and Telecommunications Press, Beijing, China, 2019.

[4] Y. Y. Hu, X. J. Li, and Y. L. Li, "Compressed sensing underwater optical communicationchannel estimation method of DCO-OFDM system," *Optical communication technology*, vol. 44, no. 7, pp. 28–31, 2020.

[5] G. W. Yang, Z. B. Huang, and B. Pan, "Indoor positioning and orientating system basedon visible light communication," *Journal on Communications*, vol. 41, no. 12, pp. 162–170, 2020.

[6] Y. Tanaka, S. Haruyama, and M. Nakagawa, "Wireless optical transmissions with whitecolored LED for wireless home links," in *Proceedings of the International Symposium on Personal Indoor and Mobile Radio Communications*, pp. 1325–1329, IEEE Press, London, UK, September 2000.

[7] T. Komine and M. Nakagawa, "Performance evaluation of visible-light wireless communication system using white LED lightings," in *Proceedings of the International Symposium on Computers and Communications*, pp. 258–263, IEEE Press, Alexandria, Egypt, July 2004.

[8] S. Rajagopal, R. Roberts, and S.-K. Lim, "IEEE 802.15.7 visible light communication: modulation schemes and dimming support," *IEEE Communications Magazine*, vol. 50, no. 3, pp. 72–82, 2012.

[9] J. Vucic, C. Kottke, S. Nerreter, and A. K.-D. J. W. Buttner, "White light wireless transmission at 200${+}$ mb/s net data rate by use of discrete-multitone modulation," *IEEE Photonics Technology Letters*, vol. 21, no. 20, pp. 1511–1513, 2009.

[10] N. Fujimoto and S. Yamamoto, "The fastest visible light transmissions of 662 Mb/s by a blue LED, 600 Mb/s by a red LED, and 520 Mb/s by a green LED based on simple OOK-NRZ modulation of a commercially available RGB-type white LED using pre-emphasis and post-equalizing techniques"" in *Proceedings of the European Conference on Optical Communication*, pp. 1–3, IEEE Press, Cannes, France, September 2014.

[11] X. Zhu, F. M. Wang, M. Shi, N. Chi, J. Liu, and F. Jiang, "10.72Gb/s visible light communication system based on single packaged RGBYC LED utilizing QAM-DMT modulation with hardware pre-equalization," in *Proceedings of the*

Optical Fiber Communication Conference, pp. 1–3, IEEE Press, San Diego, CA, USA, March 2018.

[12] C. Wang, G. Li, F. Hu, and Y. J. P. Q. J. Z. N. Zhao, "Visible light communication for Vehicle to Everything beyond 1 Gb/s based on an LED car headlight and a 2 × 2 PIN array," *Chinese Optics Letters*, vol. 18, no. 11, Article ID 110602, 2020.

[13] M. S. A. Mossaad, S. Hranilovic, and L. Lampe, "Visible light communications using OFDM and multiple LEDs," *IEEE Transactions on Communications*, vol. 63, no. 11, pp. 4304–4313, 2015.

[14] F. Hu, "20.09-Gbit/s underwater WDM-VLC transmission based on a single Si/GaAs-substrate multichromatic LED array chip," in *Proceedings of the Optical Fiber Communications (OFC) Conference, paper M3I.7*, vol. 4, p. 2020, San Diego, CA, USA, March 2020.

[15] H. Qian, S. Cai, S. Yao, T. Zhou, Y. Yang, and X. Wang, "On the benefit of DMT modulation in nonlinear VLC systems," *Optics Express*, vol. 23, no. 3, p. 2618, 2015.

[16] L. Peng, M. Helard, and S. Haese, "On bit-loading for discrete multi-tone transmission over short range POF systems," *Journal of Lightwave Technology*, vol. 31, no. 24, pp. 4155–4165, 2013.

[17] Y. F. Liu, Y. C. Chang, C. W. Chow, and C. H. Yeh, "Equalization and pre-distorted schemes for increasing data rate in in-door visible light communication system," in *Proceedings of the Optical Fiber Communications (OFC) Conference, paper JWA83*, San Diego, CA, USA, March 2011.

[18] H. Li, X. Chen, B. Huang, D. Tang, and H. Chen, "High bandwidth visible light communications based on a post-equalization circuit," *IEEE Photonics Technology Letters*, vol. 26, no. 2, pp. 119–122, 2014.

[19] Y. Yang, Z. Yuan, J. Chen, and M. Guo, "Assessment of osculating value method based on entropy weight to transportation energy conservation and emission reduction," *Environmental Engineering and Management Journal*, vol. 16, no. 10, pp. 2413–2423, 2017.

[20] Y. Yang, K. Wang, Z. Yuan, and D. Liu, "Predicting freeway traffic crash severity using XGBoost-Bayesian network model with consideration of features interaction," *Journal of Advanced Transportation*, Article ID 4257865, 2022.

[21] X. Chen, Z. Feng, M. Tang, S. Fu, and D. Liu, "Performance enhanced DDO-OFDM system with adaptively partitioned precoding and single sideband modulation," *Optics Express*, vol. 25, no. 19, p. 23093, 2017.

[22] Y. Hong, J. Xu, and L.-K. Chen, "Experimental investigation of multi-band OCT precoding for OFDM-based visible light communications," *Optics Express*, vol. 25, no. 11, p. 12908, 2017.

[23] K. Wu, J. He, J. Ma, and Y. Wei, "A BIPCM scheme based on OCT precoding for a 256-QAM OFDM-VLC system," *IEEE Photonics Technology Letters*, vol. 30, no. 21, pp. 1866–1869, 2018.

[24] M. Chen, L. Wang, D. Xi, L. Zhang, H. Zhou, and Q. Chen, "Comparison of different precoding techniques for unbalanced impairments compensation in short-reach DMT transmission systems," *Journal of Lightwave Technology*, vol. 38, no. 22, pp. 6202–6213, 2020.

[25] J. Armstrong, "OFDM for optical communications," *Journal of Lightwave Technology*, vol. 27, no. 3, pp. 189–204, 2009.

[26] J. He, J. He, and J. Shi, "An enhanced adaptive scheme with pairwise coding for OFDM-VLC system," *IEEE Photonics Technology Letters*, vol. 30, no. 13, pp. 1254–1257, 2018.

[27] Z. Feng and M. S. L. Q. R. R. P. D. Tang, "Performance-enhanced direct detection optical OFDM transmission with CAZAC equalization," *IEEE Photonics Technology Letters*, vol. 27, no. 14, pp. 1507–1510, 2015.